JOURNAL OF PROPULSION AND POWER
Vol. 23, No. 2, March–April 2007

Investigation of Spray Behavior Downstream of an Aeroengine Injector with Acoustic Excitation

P. Gajan,* A. Strzelecki,* B. Platet,* and R. Lecourt*
ONERA, 31055 Toulouse, France
and
F. Giuliani†
Graz University of Technology, 8010 Graz, Austria

DOI: 10.2514/1.22394

An experiment was developed to reproduce the effects on fuel spray behavior of large pressure and velocity fluctuations observed in a gas turbine with combustion instability phenomena. A spray produced by an air-blast atomizer was injected into a chamber closed on both sides by sonic nozzles. The pressure and velocity fluctuations were created by periodic modification of the downstream nozzle area using a cogged wheel. Phase-averaged techniques were used to monitor the air velocity field and spray pattern oscillations during the excitation cycle. The results revealed the existence of low Mach number traveling waves inside the chamber. Convection velocities of these waves were determined. The spray exhibited a droplet density wave formed mainly with smaller droplet sizes. An analysis based on experimental observations and numerical calculations showed that this wave has two origins. The first is linked to the atomization process and the second to the transport of droplets by the oscillating airflow. The existence of this wave plays an important role in the pressure and heat release coupling that is at the origin of the combustion instabilities.

Nomenclature

B_M	=	Spalding number for mass transfer around a droplet
B_T	=	Spalding number for thermal transfer around a droplet
C_d	=	drag coefficient of the droplet
c_{pl}	=	specific heat capacity of the liquid fuel, J/(kg · K)
c_{pv}	=	specific heat capacity of the vapor fuel, J/(kg · K)
d	=	droplet size, μm
d_{atomizer}	=	reference diameter of the air-blast atomizer, m
f	=	frequency, Hz
Le	=	Lewis number
Lv	=	latent heat of vaporization of the liquid fuel, J/kg
m_p	=	mass of the droplet, kg
$N(\phi, d)$	=	number of droplets in the sample belonging to the class diameter d and measured at the phase angle ϕ
Nu	=	Nusselt number
$N_T(d)$	=	total number of droplets of the size class d measured in the sample
p'	=	root mean square value of the pressure signal, Pa
q'	=	unsteady rate of heat release per unit volume, W/m^3
Sc	=	Schmidt number
Sh	=	Sherwood number used to model the heating of the droplet
Tg	=	temperature of the gas phase
Tp	=	temperature of the droplet
U	=	air velocity component in the longitudinal direction, m/s
U_c	=	convection velocity of the air velocity wave, m/s
U_o	=	reference velocity calculated from the mass flow rate and the reference diameter, m/s
$U_{p_{\mathrm{conv}}}$	=	convection velocity of the droplet density wave, m/s
u'	=	root mean square value of the velocity signal, m/s
$\boldsymbol{V}_g$	=	gas velocity, m/s
$\boldsymbol{V}_p$	=	velocity of the droplet, m/s
v'	=	acoustic velocity, m/s
$x; y; z$	=	spatial coordinates, m
y_g	=	mass fraction of fuel vapor in the droplet neighborhood
y_s	=	mass fraction of fuel vapor on the droplet surface
λ_g	=	thermal conductivity of the gas, W/(m · K)
μ_g	=	dynamic viscosity of the gas, N · s/m^2
ρ_g	=	gas density, kg/m^3
ρ_l	=	liquid-fuel density, kg/m^3
ϕ	=	phase angle, rad
$\chi(d)$	=	droplet concentration parameter

Introduction

COMBUSTION instabilities are observed in many applications, from domestic boilers to rocket thrusters or aeronautics combustors. They result from a coupling between the acoustic pressure and velocity field and the unsteady rate of heat release by the heat source. This coupling induces a great amplification of the pressure and temperature oscillations that can provoke mechanical damage to the chamber. Although these phenomena have been observed for more than a century, the mechanisms linking the acoustic pressure or velocity fluctuations to the unsteady heat release of the flame are not clear in all configurations and many studies are still being performed.

For aeroengine applications, recent economic and environmental requirements have led to the development of new combustor concepts with shorter length, higher pressure, and operating in lean combustion regimes in order to limit NOx formation. In these new chambers, a maximum airflow rate is needed for the fuel injection and less air is available for the dilution. Consequently, a multiperforation technique is used for the wall cooling, resulting in greater acoustic impedance of the walls. All these geometric modifications enhance the appearance of combustion instabilities,

Received 11 January 2006; revision received 6 July 2006; accepted for publication 7 July 2006.

*Research Engineer, Centre de Toulouse, Models for Aerodynamics and Energetics Department, 2 Avenue Edouard Belin.

†Research Scientist, Institute for Thermal Turbomachinery and Machine Dynamics, Inffeldgasse 25A.

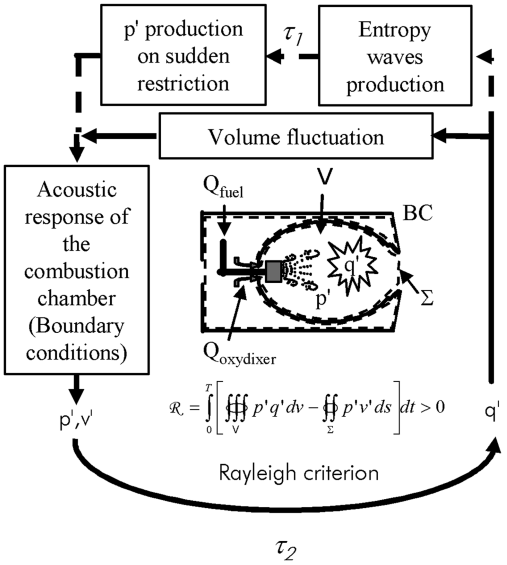

Fig. 1 Diagram of the acoustic/heat release coupling appearing in the event of combustion instabilities.

and research programs have been conducted in order to improve the understanding of the mechanism involved and to develop calculation techniques for predicting them.

The acoustic/heat release coupling can be described as a closed loop, as shown in Fig. 1. On the upper branch of the loop, the production of pressure or velocity fluctuations by the flame has been studied by many authors and a description of the different phenomena involved can be found in Ducruix et al. [1] and Lieuwen [2]. Similarly, different authors [3,4] show that pressure fluctuations can arise when entropy waves, issued from the unsteady heat release, interact with an abrupt modification to the cross section (nozzle). Note that in most cases, the Mach number in the chamber being low, the entropy wave convection induced a large time delay between the unsteady heat release and induced pressure fluctuations in comparison with the time scale associated with the direct acoustic perturbation produced by the flame.

On the other branch of the loop, the production of heat release from p' or v' is not so clear [1] and depends on the characteristics of the combustion system. A lot of basic work has been performed on gas-fueled combustion devices (premixed or not) in order to describe the phenomena involved and to determine their characteristics in terms of time delay and amplitude [5–14].

A detailed description of these phenomena and, in particular, the determination of the different amplitude and phase relationships between each of them (transfer function) is necessary to define through the Rayleigh criterion (Fig. 1), the amplification ($\mathcal{R} > 0$), or the attenuation of the oscillations ($\mathcal{R} < 0$) and thus to determine, for a given chamber, the risk of a combustion instability occurrence.

Combustion instabilities being also observed in liquid-fueled combustion chambers, authors have performed some basic experiments [15,16] in order to understand the specific phenomena linked to liquid-fuel injection. Eckstein et al. [16] analyzed the spray issued from an air-blast system submitted to periodic air velocity fluctuations. In their experiments, these fluctuations were produced by a siren placed upstream of the injector. They observed that the droplet size in the spray varied periodically at the same frequency as the velocity excitation. Eckstein et al. explained that, for a given liquid flow rate, high air velocities produce a large number of small droplets, whereas low air velocities produce a small amount of large droplets. In this way, when combustion instability occurs, the periodic velocity fluctuations inside of the atomizer create a time-varying droplet size distribution that is transported further downstream toward the flame as a wave. During this convection phase, the small droplet zones produce a larger amount of fuel vapor than the large-droplet zones. As a result, an equivalence ratio wave appears that interacts with the flame to produce a periodic heat release oscillation.

In parallel, Giuliani et al. [15] studied spray behavior downstream of a simplified liquid-fueled atomizer with no prefilming zone where the droplets are formed from the disintegration of an axisymmetrical liquid sheet sheared internally and externally by two coswirling airflows. When they pulsed the airflow rate with a siren placed upstream of the injector, they observed the appearance of a droplet density wave transported downstream of the atomization zone. Droplet size measurements performed with a Fraunhofer–Mie light scattering method showed that the local droplet density waves were mainly linked to an oscillation of the number of small droplets in the histogram. By using a one-dimensional model based on the Boussinesq–Basset–Oseen (BBO) transport equation [15], they concluded that this observation is due to the influence of the oscillating velocity field on the motion of the small droplets, which segregates them in space and, therefore, forms the droplet concentration waves observed. From different isothermal experiments at room conditions, they noted that the droplet classes involved had a Stokes number calculated from the air velocity frequency, inferior to 0.2.

The results presented in this paper concern an analysis of the air and liquid behavior downstream of an air-blast atomizer placed in a chamber submitted to realistic pressure fluctuations. Detailed gas velocity and spray characterizations are reported in order to analyze the influence of the pressure and velocity fluctuations on the two-phase flowfield.

Experimental Setup

The experiments were performed on a tubular combustion chamber equipped with a Dextre-type atomizer (Fig. 2). The inlet air is heated by an electrical exchanger. The dimensions of the combustion chamber are $129 \times 129 \times 284$ mm. The coordinate origin is located on the test section centerline, in the outlet plane of the atomizer.

The test section is delimited on both sides by critical nozzles. On the outlet, the surface area of the nozzle can be periodically changed by the teeth of a rotating cogged wheel. Because the inlet mass flow rate is imposed by the upstream choked nozzle, the variation of this surface induces pressure and velocity fluctuations in the chamber.

The experiments were performed without combustion, using ethanol as the liquid. The surface tension and density of this fluid are equivalent to kerosene and so its disintegration gives a similar spray behavior. The excitation frequency is controlled by a signal delivered by an optoelectronic sensor placed on the cogged wheel.

Three types of measurements were performed. First, the acoustic characterization of the installation was carried out with a B&K microphone. This work permitted us to determine the acoustic modes of each part of the installation. Then a laser Doppler anemometer (LDA) was used to define the airflow characteristics in the combustion chamber. In the same way, a phase Doppler analyzer (PDA) gave the droplet size and velocity distribution downstream of the atomizer. A phase-averaged technique was applied on both

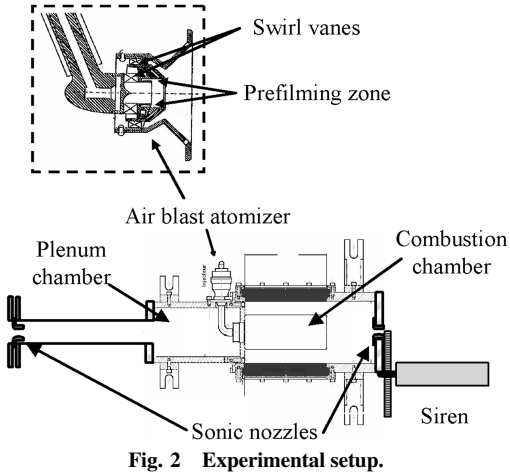

Fig. 2 Experimental setup.

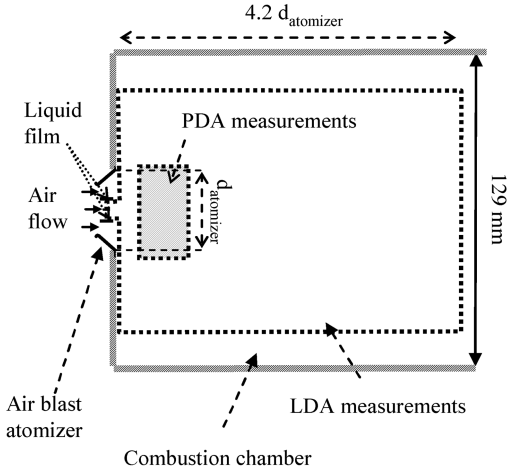

Fig. 3 Diagram of the experimental arrangement; $d_{in}/d_{atomizer} = 0.27$ and $d_{out}/d_{atomizer} = 0.64$.

systems in order to monitor the evolution of the air velocity field and liquid phase characteristics through one pulsation period [17].

LDA and PDA measurements were performed for different excitation frequencies. LDA measurements were performed without liquid injection. They gave the three velocity components in different planes situated between the inside of the atomizer and a cross section of the combustion chamber located 4.2 times a reference diameter (that of the outer diameter of the atomizer: $d_{atomizer}$) downstream of the injection device exit (Fig. 3). The velocity measurements inside of the atomizer enabled us to define the airflow conditions close to the film disintegration zone. PDA measurements were performed in a different plane located from 0.3 to 1 $d_{atomizer}$ downstream of the injector.

Experimental Results

Characteristics of the Acoustic Field

In a first step, this characterization was performed without flow in cold conditions. The two nozzles were closed and the test section was equipped with translation systems for moving the microphone sensor in the combustion chamber. The chamber was placed in a reverberant room and excited by a high-level white noise produced by a loudspeaker. The pressure spectra (Fig. 4) showed different frequencies corresponding to the respective longitudinal and transverse modes of the combustion chamber and the plenum chamber. The peak observed at low frequency corresponds to a coupling mode between the two chambers through the nozzle formed

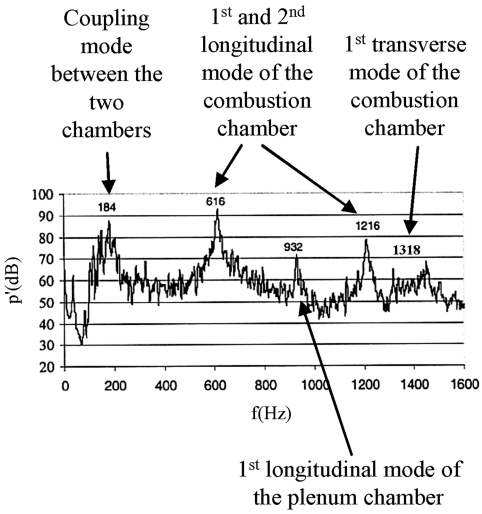

Fig. 4 Pressure spectrum measured in the combustion chamber without flow and with a white noise excitation; $y/d_{atomizer} = 0.61$.

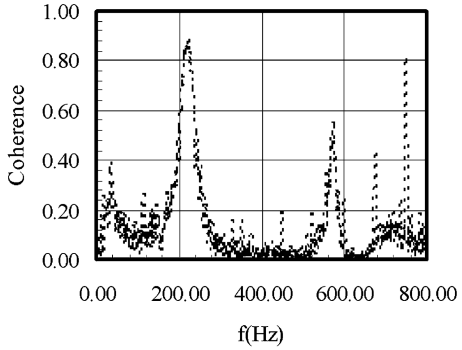

Fig. 5 Coherence function between pressure signals measured in steady flow upstream and downstream of the injection device.

by the atomizer. This mode was also observed with flow on the coherence function between pressure signals measured upstream and downstream of the injection system with an airflow but without excitation (Fig. 5).

When exciting the flow with a frequency corresponding to the first longitudinal mode of the combustion chamber, the pressure fluctuation amplitude reached 1.25% of the absolute combustion chamber pressure. Equivalent levels were obtained in combustion chambers submitted to combustion instabilities [16,18].

Air Velocity Field

LDA measurements performed at different excitation frequencies revealed that the fluctuation rates depend on the frequency. Large fluctuations were obtained at low frequency (around 50 Hz) and for the first longitudinal mode of the combustion chamber (around 700 Hz at the operating temperature). For this mode, the rms amplitude of the volume flow rate reaches 30% of the mean value in the plane of the atomizer exit. A detailed description of the flowfield obtained downstream of a simplified air-blast system in pulsed conditions [15,17] indicated that the flow pattern is dominated by two phenomena: Close to the chamber axis, a central recirculation zone oscillates with a backward and forward motion, and on the jet periphery, ring vortices are periodically detached and convected further downstream. The velocity field obtained downstream of the Dextre injector is quite similar. In particular, the oscillating backward and forward motion of the central recirculation zones is observed near the atomizer exit. The amplitude of this oscillation can be visualized by the longitudinal distributions of the axial velocity on the chamber centerline for different phase angles (Fig. 6). The oscillation observed on these distributions corresponds to a forward propagation of a velocity wave. This phenomenon is clearly observed in Fig. 7, where phase-averaged axial velocity signals measured on the chamber axis are plotted for three planes from the inside of the injector to the $0.45d_{atomizer}$ downstream. Such phase delay is also obtained on the instantaneous volume flow rate signals deduced from the phase-averaged velocity profiles measured in each section. The phase delay between these signals corresponds to a convective phenomenon with a characteristic velocity equal to 1.14 times the reference velocity. This reference velocity is calculated from the mass flow rate in the chamber, the air density and the reference diameter. It might seem surprising to obtain a convection velocity greater than the reference velocity. Nevertheless, due to the swirl effect, the axial velocity profiles exhibit, on the periphery, high-velocity zones up to three times the reference velocity (Fig. 8).

The phase-averaged velocity profile plotted in Fig. 8 shows that for $y/d_{atomizer}$ equal to -0.12, the flow in the central part of the injector has a synthetic jet-type behavior with zero mean mass flux. Furthermore, very large periodic velocity fluctuations exist near the prefilming zone where the disintegration of the liquid film occurs (Fig. 3).

Spray Behavior

The phase-averaged technique applied to PDA measurements allows monitoring of the evolution of droplet velocity and population

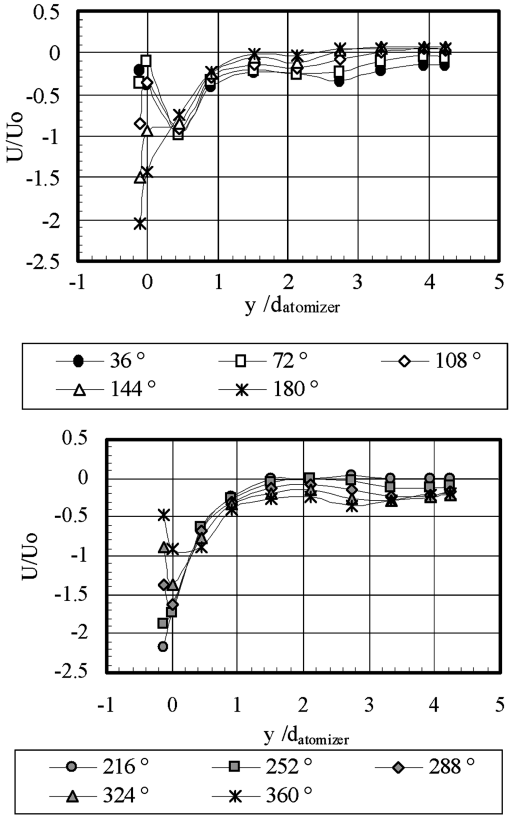

Fig. 6 Centerline velocity distribution in the chamber for different phase angles.

distribution during the excitation cycle. A typical three-dimensional plotting of the results obtained on one measurement point is shown in Fig. 9. In this figure, the gray levels correspond to the axial velocity of the droplets. This figure shows that the excitation imposes an important modulation of the number of droplets during the cycle, mainly for small droplet sizes. Furthermore, the gray level mapping reveals that the maximum velocity zone is reached between the minimum and the maximum of the droplet population.

From these raw results, it is possible to extract individual phase-averaged signals (velocity and population) for each class of droplet size, and to monitor their respective spatial evolution. In Fig. 10, normalized velocity signals obtained on different sections for two classes of droplet size are plotted. This figure exhibits a phase delay from one section to the next, which corresponds to a convective phenomenon. Furthermore, the comparison between the two graphs indicates that these delays depend on the droplet size. Its evolution along the *y* axis with respect to the droplet size is plotted in Fig. 11. A quasi-linear increase of this delay is obtained and an averaged convection velocity is calculated (Fig. 12). This figure indicates that

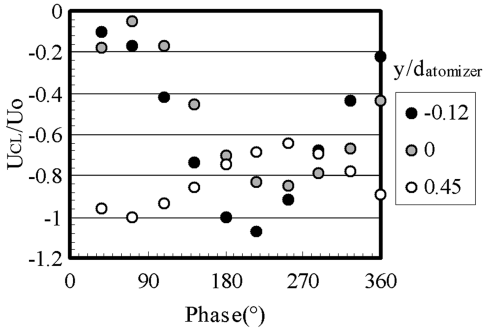

Fig. 7 Evolution of the axial velocity on the centerline during the pulsation cycle and influence of the longitudinal location; $f = 700$ Hz and $\Delta P/P = 2\%$.

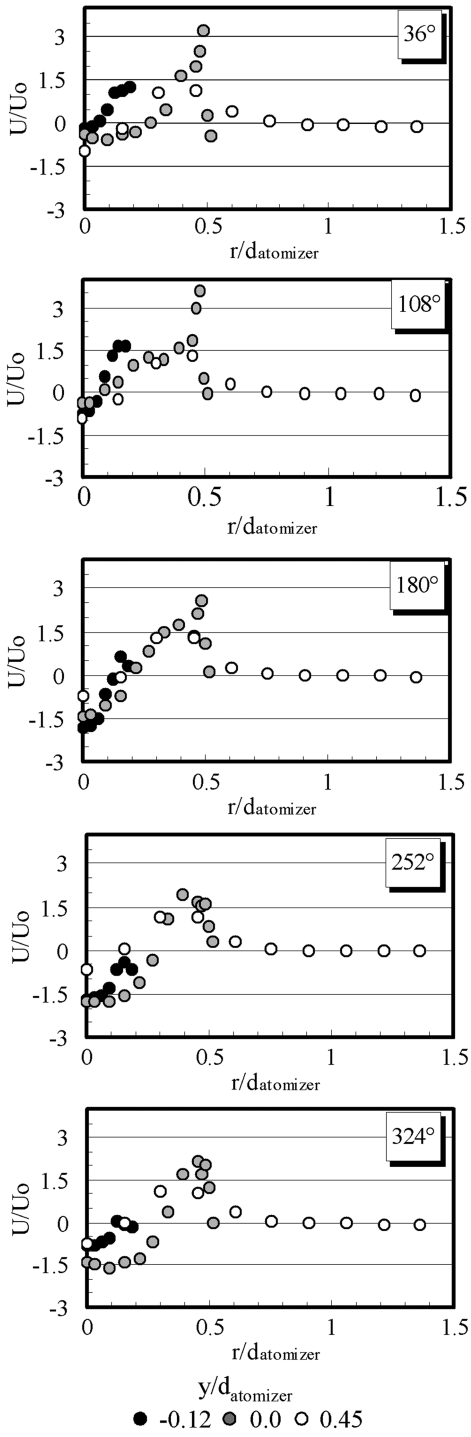

Fig. 8 Evolution of the axial velocity profiles of the airflow inside and downstream of the air-blast injector; $f = 700$ Hz and $\Delta P/P = 2\%$.

the convection velocity of the wave increases with the droplet size. So, in the chamber, the large droplets conserve their initial velocity reached near the injector exit, whereas the small droplets follow the air deceleration due to the jet expansion.

To monitor the spray population in space during the excitation cycle, the following parameter is defined:

$$\chi(\phi, d) = \frac{N(\phi, d)}{N_T(d)}$$

The phase-averaged evolution of this parameter during the excitation cycle is plotted in Fig. 13 for the smaller droplet class. This graph shows that the spray is traversed by a droplet concentration wave that propagates from the injector toward the exit of the chamber.

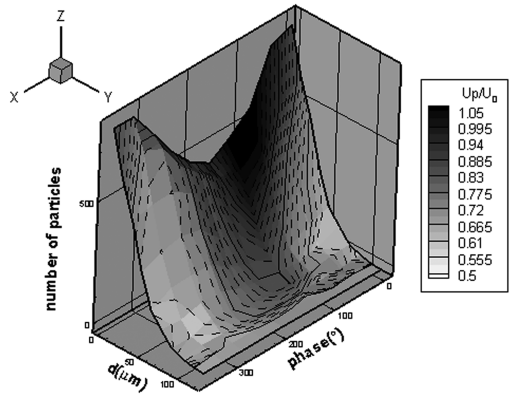

Fig. 9 Evolution of the droplet size histogram along the pulsation cycle gray levels correspond to the droplet velocity in the longitudinal direction; $f = 700$ Hz, $x/d_{\text{atomizer}} = -0.45$ $y/d_{\text{atomizer}} = 0.45$, and $z/d_{\text{atomizer}} = 0$.

Furthermore, this wave is amplified during its convection. In Fig. 14, the amplitude of the droplet concentration wave is plotted with respect to the y coordinate and the droplet size class. It confirms the amplification of this wave. Nevertheless, this amplification concerns mainly the small droplets. Two mechanisms can explain this result.

First, as mentioned previously by Eckstein et al. [16], this wave results from the liquid sheet disintegration by the oscillating airflow. Indeed, it is well known that the atomization rate and the droplet size

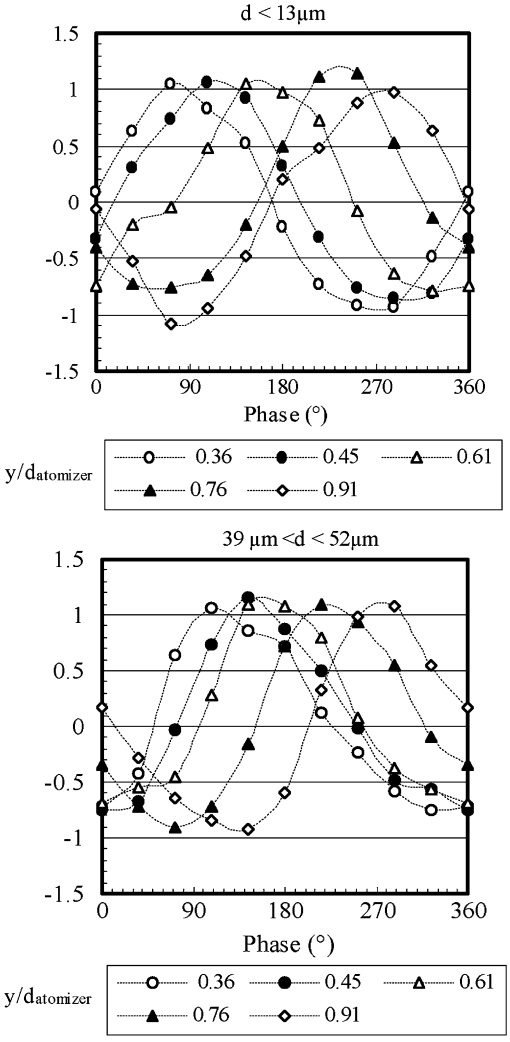

Fig. 10 Droplet velocity signals with respect to their size and their position in the chamber.

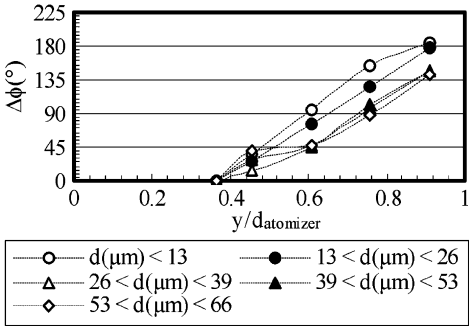

Fig. 11 Analysis of the phase delay between the droplet velocity signals with respect to their size and their position in the chamber.

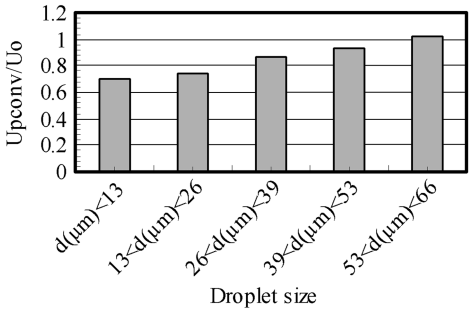

Fig. 12 Averaged convection velocity of the droplet density waves with respect to their size.

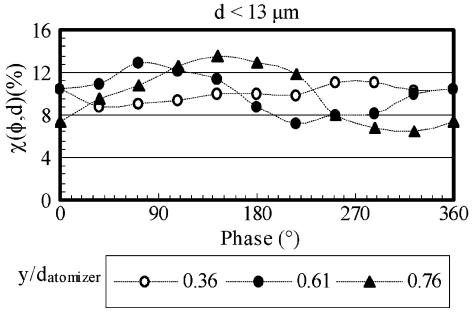

Fig. 13 Signals of number of droplets measured in different locations downstream of the atomizer.

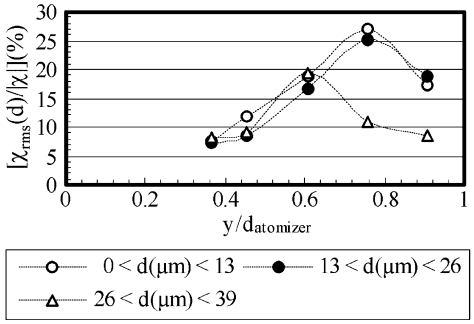

Fig. 14 Amplitude of the number of droplets wave at different locations with respect to the droplet size.

of a liquid film is greatly dependent on airflow velocity. Work on atomization of film in pipes shows that the atomization rate is, on average, proportional to the square root of the bulk velocity [19–21]. At the same time, the mean droplet size produced by liquid sheet disintegration is roughly inversely proportional to the gas velocity [22]. To examine the influence of this mechanism, it is possible to compare the air velocity signal measured close to the liquid film

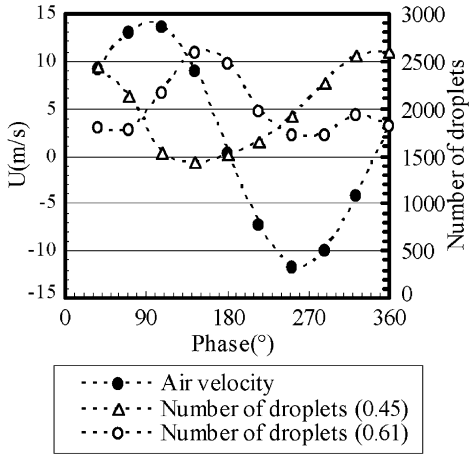

Fig. 15 Comparison between the air velocity oscillation signal measured close to the liquid film disintegration zone ($r/d_{\text{atomizer}} = 0.12$ and $y/d_{\text{atomizer}} = -0.18$) and the number of droplets measured further downstream.

atomization zone with the droplet concentration waves measured downstream (Fig. 15). This figure shows that a phase delay appears between the velocity and the number of droplet signals measured downstream of the atomizer. This delay corresponds to the convection time of the droplet concentration wave between the atomization zone and the measurement point. This time delay gives a convection velocity of the wave equal to $0.5\,U_o$.

The second mechanism that may contribute to the formation of concentration waves is the transport of the droplets by an oscillating convective velocity wave. This phenomenon, also observed by Giuliani et al. [15], will be analyzed in greater detail in this paper. For this purpose, we performed a one-dimensional calculation to simulate droplet behavior in the spray. This calculation is based on the transport equation of isolated spherical particles by a gas flow. Because the density ratio between the gas and the liquid is small, several terms can be neglected and the equation can be reduced to

$$\frac{\mathrm{d}\boldsymbol{V}_p}{\mathrm{d}t} = \frac{3}{4}\frac{\rho_g}{\rho_l}\frac{C_d}{d}\|\boldsymbol{V}_g - \boldsymbol{V}_p\|(\boldsymbol{V}_g - \boldsymbol{V}_p)$$

where C_d depends on the Reynolds number based on the slip velocity.

For this calculation, the following traveling wave equation is taken into account for the gas velocity.

$$V_g(x,t) = U_g(x)\left\{1 + \frac{u'}{U_g(x)}\sin\left[2\pi f\left(t - \frac{x}{U_c}\right)\right]\right\}$$

The first right-hand side term $U_g(x)$ simulates the air velocity deceleration downstream of the atomizer. It was defined from the flow measurements. Furthermore, an evaporation model is used to calculate the droplet size modifications. This model takes into account the droplet heating due to convection heat flux from the gas phase. The following equation is solved at each time step:

$$\frac{\mathrm{d}(d^2)}{\mathrm{d}t} = -K^{\mathrm{ev}}$$

The coefficient K^{ev} depends on the droplet and gas properties.

$$K^{\mathrm{ev}} = \frac{\mu_g Sh}{\rho_l Sc}\ell_n(1 + B_M)$$

In this equation, Sh depends on the Reynolds number. It takes into account the influence of the convective phenomena on the evaporation [23]. B_M is based on the vapor concentration difference $(y_s - y_g)$ between the droplet surface and its environment.

$$B_M = \frac{y_s - y_g}{1 - y_s}$$

In these calculations, the K^{ev} factor increases with the slip velocity between the droplets and the gas and the liquid temperature through the saturated vapor pressure at the droplet surface.

For this purpose, the droplet temperature is calculated from the following balance equation:

$$m_p c_{pl}\frac{\mathrm{d}T_p}{\mathrm{d}t} = \pi Nu\lambda_g\,\mathrm{d}(T_g - T_p)\frac{\ell_n(1 + B_T)}{B_T} + \frac{\mathrm{d}m_p}{\mathrm{d}t}L_v(T_p)$$

In this equation, Nu is calculated from the Ranz–Marshall correlation, and B_T is a nondimensional term describing the thermal flux exchanges. Given certain hypotheses, this new term can be deduced from the previous Spalding number using the following expression:

$$B_T = (1 + B_M)^{\alpha} - 1 \quad \text{with } \alpha = (c_{\mathrm{pv}}/c_{\mathrm{pg}})Le$$

Generally, the Lewis number is around one.

The calculations were performed with an explicit method with a time step equal to 7×10^{-5} the period of the excitation. Periodically, droplets of different sizes are injected at zero velocity at the origin point.

Figure 16 corresponds to the size and location of the injected droplets, 2 ms after the beginning of the calculation. It clearly shows that the oscillating airflow imposes a spatial segregation of the droplets, in particular, for the smaller ones. We can also notice that, for small droplets, large size variations are predicted in dense zones. This means that the vapor production mainly appears in these regions.

From postprocessing, it is possible to calculate the droplet number and droplet velocity signal at a given location for different droplet sizes. An example of this treatment is shown in Fig. 17. It indicates that the two waves are not in phase. Furthermore, the concentration signal obtained from the simulation is not sinusoidal. A similar result is obtained experimentally close to the injector. The phenomena observed for the smaller droplets have some similarities with the klystron effect described by Harrje and Reardon [24] for liquid propellant rockets. This effect, imposed by liquid flow rate oscillations, corresponds to a bunching of the liquid phase at a location downstream of the injector. In our work, the unsteady drag forces induced by the air velocity oscillations impose, for a given droplet size class, different time-averaged flight velocities. Hence, as faster particles catch up with the slower ones, droplets gather in space. Nevertheless, further downstream, the droplet concentration peak diffuses and the signal becomes more sinusoidal (Fig. 13).

In Fig. 18, the spatial evolution of the droplet concentration signal is shown. An amplification of the wave is thus observed, confirming the experimental results. This spatial evolution of the amplitude with respect to droplet size is plotted in Fig. 19. The model predicts that this amplification concerns the smaller droplets. For the flow conditions considered, the concentration waves are not further amplified for droplet sizes greater than 65 μm. Comparison between

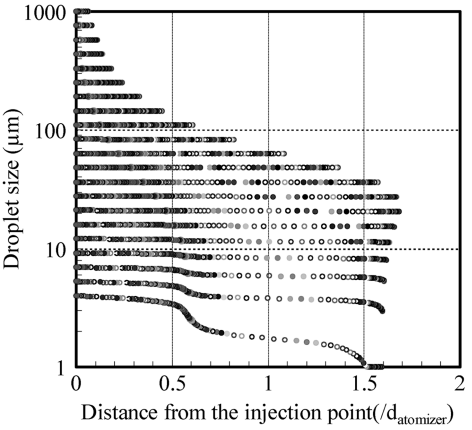

Fig. 16 Instantaneous droplets position and size obtained from the numerical simulation.

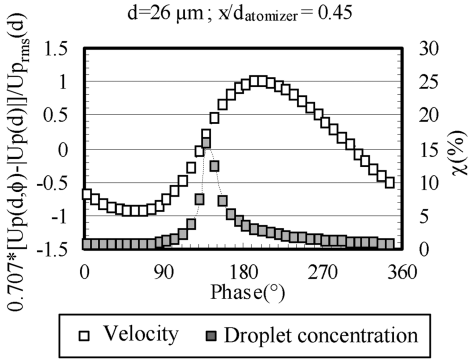

Fig. 17 Velocity and droplet concentration signals calculated downstream of the injection point for one class of droplet size.

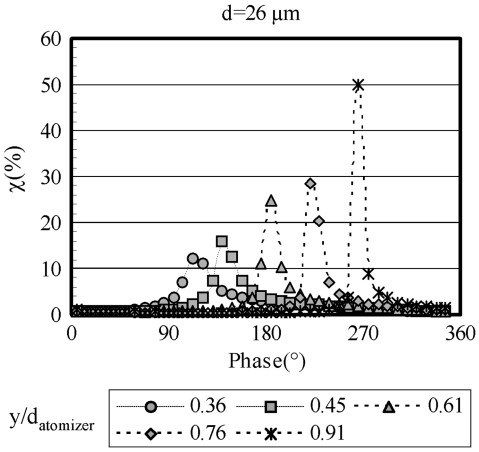

Fig. 18 Droplet concentration signals calculated at different distances from the injection point for one class of droplet size.

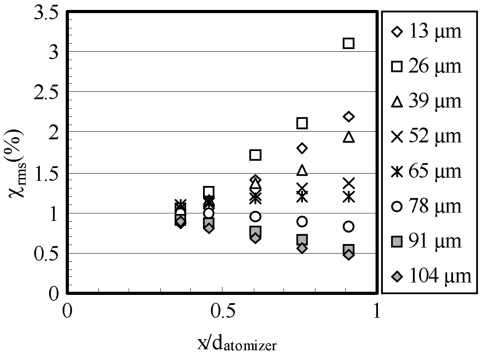

Fig. 19 Amplitude of the droplets concentration wave at different locations with respect to the droplet size.

experimental and numerical results (Figs. 14 and 19, respectively) shows that the amplification rate is largely overestimated. This discrepancy is due to the simplicity of the numerical method used here to understand the experimental observations.

From this analysis, it is possible to conclude that the large air velocity fluctuations imposed by the excitation creates a droplet density wave that is transported from the injector to the combustion zone. This wave has two origins. The first is linked to the atomization process of the liquid film in the atomizer and the second is related to the transport of the droplet by the convective wave. These two mechanisms will play an important role in the $p'q'$ coupling leading to combustion instabilities. Nevertheless, in order to fully understand this coupling, it will be necessary to study in more detail the transformation of the droplet density wave into an equivalent-ratio wave that will directly interact with the flame to produce heat release fluctuations.

Conclusions

The development of predictive methods for avoiding the appearance of combustion instabilities in future aeroengine combustors first requires a full understanding of the different mechanisms occurring in $p'q'$ coupling. Many of them were previously described in the past. Nevertheless, for liquid-fueled combustors, some specific phenomena exist that have an important effect on dynamic combustor behavior. The objective of the work presented in this paper is to examine them experimentally.

The results show that when the pressure oscillations in the chamber are sufficiently high, the air velocity fluctuations linked to these oscillations provoke a droplet density wave that is transported toward the combustion zone. The coupling between the air velocity wave and the spray behavior was demonstrated by a simple one-dimensional calculation based on the transport and evaporation equations of droplets. The convection velocity of this wave and the position of the flame impose a time-lag distribution between the pressure and heat release fluctuations. As shown by many authors, this time delay distribution is an important factor that controls the appearance of combustion instabilities. The transformation of this wave into an equivalent-ratio wave through evaporation and mass diffusion processes is unclear and will need some new experimental and numerical developments in the future. These processes will control the amplitude of the equivalent-ratio fluctuations interacting with the flame and, consequently, the amplitude of the heat release fluctuation.

Acknowledgments

The air velocity and droplet size measurements were performed by Alain Bontemps. The test facility was modified by André Alcoser. The authors would like to thank them for their useful help.

References

[1] Ducruix, S., Schuller, T., Durox, D., and Candel, S., "Combustion Dynamics and Instabilities: Elementary Coupling and Driving Mechanisms," *Journal of Propulsion and Power*, Vol. 9, No. 5, Oct. 2003, pp. 722–734.

[2] Lieuwen, T., "Modeling Premixed Combustion-Acoustic Wave Interactions: A Review," *Journal of Propulsion and Power*, Vol. 9, No. 5, Oct. 2003, pp. 765–781.

[3] Marble, F. E. and Candel, S. M., "Acoustic Disturbance from Gas Non-Uniformities Convected Through a Nozzle," *Journal of Sound and Vibration*, Vol. 55, No. 2, 1977, pp. 225–243.

[4] Polifke, W., Paschereit, C. O., and Döbbeling, K., "Constructive and Destructive Interference of Acoustic and Entropy Waves in a Premixed Combustor with a Choked Exit," *International Journal of Acoustics and Vibration*, Vol. 6, No. 3, 2001, pp. 135–146.

[5] Poinsot, T. J., Trouve, A. C., Veynante, D. P., Candel, S. M., and Esposito, E. J., "Vortex-Driven Acoustically Coupled Combustion Instabilities," *Journal of Fluid Mechanics*, Vol. 177, Apr. 1987, pp. 265–292.

[6] Candel, S., and Poinsot, T., "Interactions Between Acoustics And Combustion," *Proceedings of the Institute of Acoustics*, Vol. 10, 1988, pp. 103–154.

[7] Schadow, K. C., Gutmark, E., Parr, T. P., Parr, D. M., and Wilson, K. J., "Large-Scale Coherent Structures as Drivers of Combustion Instability," *Combustion Science and Technology*, Vol. 64, No. 4-6, 1989, pp. 167–186.

[8] Heneghan, S., Lesmerises, A. L., and Sturgess G. J, "Acoustic Characteristics of a Research Step Combustor," AIAA Paper 90-1851, 1990.

[9] Candel, S. M., "Combustion Instabilities Coupled by Pressure Waves and Their Active Control," *24th Symposium (International) on Combustion*, The Combustion Institute, Pittsburgh, PA, 1992, pp. 1277–1296.

[10] Shih, W. P., Lee, J., and Santavicca, D., "Stability and Emissions Characteristics of a Lean Premixed Gas Turbine Combustor," *26th Symposium (International) on Combustion*, The Combustion Institute, Pittsburgh, 1996.

[11] Edwards, N. R., McIntosh, A. C., and Brindley, J., "The Development of Pressure Induced Instabilities in Premixed Flames," *Combustion Science and Technology*, Vol. 99, No. 1-3, 1996, pp. 373–386.

[12] Lieuwen, T., and Zinn, B. T., "The Role of Equivalent Ratio

Oscillations in Driving Combustion Instabilities in Low NOx Gas Turbines," *27th Symposium (International) on Combustion*, The Combustion Institute, Pittsburgh, 1998, pp. 1809–1816.

[13] Lee, J. G., Kim, K., and Santavicca, D. A., "Measurement of Equivalence Ratio Fluctuation and its Effect in Heat Release During Unstable Combustion," *28th Symposium (International) on Combustion*, The Combustion Institute, Pittsburgh, 2000, pp. 415–421.

[14] Dowling, A. P., and Hubbard, S., "Instability in Lean Premixed Combustors," *Journal of Power and Energy*, Vol. 214, No. A4, 2000, pp. 317–332.

[15] Giuliani, F., Gajan, P., Diers, O., and Ledoux, M., "Influence of Pulsed Entries on a Spray Generated by an Airblast Injection Device: An Experimental Analysis on Combustion Instability Processes in Aeroengines," *29th Symposium (International) on Combustion*, The Combustion Institute, Pittsburgh, 2002, pp. 91–98.

[16] Eckstein, J., Freitag, E., Hirsch, C., and Sattelmayer, T., "Experimental Study on the Role of Entropy Waves in Low Frequency Oscillations in a RQL Combustor," *Journal of Engineering for Gas Turbines and Power*, Vol. 128, No. 2, 2006, pp. 264–270.

[17] Giuliani, F., Diers, O., Gajan, P., and Ledoux, M., "Characterization of an Air-Blast Injection Device with Forced Periodic Entries," *Proceedings of the IUTAM, Symposium on Turbulent Mixing and Combustion*, edited by A. Pollard and S. Candel, Kluwer, Dordrecht, The Netherlands, 2002.

[18] DeLaat, J. C., Breisacher, J., Saus, J. R., and Paxson, D. E., "Active Combustion Control for Aircraft Gas Turbine Engines," AIAA Paper 2000-3500, 2000.

[19] Hewitt, G. F., and Govan, A. H., "Phenomenological Modelling of Non Equilibrium Flows with Phase Change," *International Journal of Heat and Mass Transfer*, Vol. 33, No. 2, 1990, p. 229.

[20] Nigmatulin, R. I., Nigmatulin, B. I., Khodzhaev, Ya. D., and Kroshilin, V. E., "Entrainment and Deposition Rates in a Dispersed-Film Flow," *International Journal of Multiphase Flow*, Vol. 22, No. 1, 1996, p. 19.

[21] Lopez de Bertodano, M. A., Assad, A., and Beus, S. G., "Experiments for Entrainment Rate of Droplets in The Annular Regime," International Journal of Multiphase flows, Vol. 27, No. 4, 2001, pp. 685–699.

[22] Lefebvre, A. H., *Atomization and Sprays*, Hemisphere, New York, 1989.

[23] Abramzon, B., and Sirignano, W. A., "Droplets Vaporization Model for Spray Combustion Calculations," *International Journal of Heat and Mass Transfer*, Vol. 32, No. 9, 1989, pp. 1605–1618.

[24] Harrje, D. T., and Reardon, F. H., "Liquid Propellant Rocket Combustion Instability," NASA SP-194, 1972.

T. Lieuwen
Associate Editor